

Solar Control Dispersions and Coatings With Rare-Earth Hexaboride Nanoparticles

Hiromitsu Takeda, Hiroko Kuno, and Kenji Adachi[†]

Ichikawa Research Laboratories, Sumitomo Metal Mining Co. Ltd., 3-18-5 Nakakokubun, Ichikawa, Chiba 272 8588, Japan

Nanoparticle dispersions of rare-earth hexaborides have been prepared using a media agitation mill and have been examined for optical properties. High visible light transmittance coupled with strong absorption in the near-infrared (NIR) wavelengths suitable for solar control windows are reported for hexaboride nanoparticle dispersions with particle size dependence and the effect of artifacts. Nanoparticulate LaB₆ shows the largest NIR absorption among rare-earth hexaborides. NIR absorption is considered to arise from the free electron plasmon resonance. On decreasing the particle size below 120 nm, both visible light transmittance and NIR absorption are found to increase gradually until the size of 18–26 nm when they reach the maximum, and then decrease again at below 18 nm. Zirconia contamination and formation of lanthanum oxide were found to be involved during the milling process, leading to small additional absorptions around 300 and 650 nm, respectively.

I. Introduction

THERE has been a growing demand in recent years to filter out the infrared waves of the solar spectrum from housing and automotive windows,¹ in accordance with the worldwide energy-saving and environmental preservation movement. By reducing the near-infrared (NIR) wavelengths between 780 and 2500 nm, it would be possible to moderate skin irritation under the strong summer sun without losing brightness. Additionally, this would help to reduce the energy for air conditioning and thereby decrease the emission of carbon oxides from housings and automobiles. The attainable driving distance of electric vehicles would also be directly increased by the NIR filters, which considerably reduce the consumption of battery energies. A major practical means to meet these demands includes conventional heat-absorbing glasses, heat-reflecting glasses, and sputtered-coating glasses among others. However, each has its own shortcomings, naturally, and the satisfactory answer to these demands is yet to be fully obtained. For example, a variety of custom colors is difficult in heat-absorbing glasses, a high luminous transparency is sacrificed in metal-coated heat-reflecting glasses, and low productivity and high cost always persist in the vacuum process solutions.

The application of nanoparticles, on the other hand, is a unique approach to reduce solar heat, as it provides a potentially low-cost and high-productivity solution. Not only does it meet mass-production requirements but also realizes high optical selectivity, i.e., a high luminous transparency at a given heat-shielding effect. A well-known material species to serve the purpose is represented by the nanoparticles of transparent oxide conductors such as tin-doped indium oxide² (ITO) and antimony-doped tin oxide³ (ATO). They are known to provide

highly transparent solar filters to absorb infrared rays by possibly activating surface plasmon polaritons of free electrons, as typically observed in gold and silver colloids.^{4,5} On the other hand, lanthanum hexaboride, a violet–black material as a powder, has also been found^{6–8} to be one of the commercial species serving as a NIR filter with high visible light transmittance. Although LaB₆ nanoparticles are finding wide commercial applications in transparent solar control substances such as PET films and PVB interlayers⁹ for automotive and architectural windows, fundamental material aspects of LaB₆ dispersions have not yet been reported. Therefore, the present paper reports the preparation and processing, the basic material properties, and the practical optical properties of lanthanum and other rare-earth hexaboride nanoparticle dispersions for solar control applications.

II. Experimental Procedure

99.9% purity powders of rare-earth oxides X₂O₃ (X = La, Ce, Pr, Nd, Gd) and boron carbides (B₄C) are mixed well and heated in vacuum at 1500°C for 3 h to obtain raw rare-earth hexaboride powder a few micrometers in size. The raw XB₆ powder is mixed with a high polymer dispersant in a solvent toluene and dispersed in a media agitation mill, such as a bead mill and a paint shaker mill, with 0.3 mm YTZ beads made of partially stabilized ZrO₂ containing 5 wt% Y₂O₃. Considering the extremely high microhardness (2770 kg/mm²) of LaB₆,¹⁰ initial trials were carried out to use a plasma reactor to obtain nanosized raw primary LaB₆ particles, but besides the poor production rate, the resulting particles were strongly coagulated and required the same lengthy pulverization process to obtain nanodispersions. Attempts were also made to utilize contamination-free milling methods such as a selfcollision-type mill and a high-energy ultrasonic mill, but neither was found to be effective in pulverizing and reducing the particle size of hard LaB₆. Thus, we have followed the media agitation mill using YTZ beads, which showed the highest efficiency in reducing the size of LaB₆ particles down to nanoscale.

The particle size and distribution in dispersions have been evaluated by a particle analyzer (Microtrack (Nanotrak) model UPA-150, Nikkiso Inc., Higashimurayama-shi, Tokyo, Japan), which is based on the dynamic light scattering method with a semiconductor laser of wavelength 780 nm and can measure undiluted high-concentration liquids. This apparatus gave almost the same average particle size values as those observed by transmission electron microscopy (TEM) (model HF 2200, Hitachi High-Technologies Corp., Minato-ku, Tokyo, Japan).

Nanoparticle dispersions were mixed with a UV-curing organic binder (UV-3701 of Toa Gosei Co., Ltd., Minato-ku, Tokyo, Japan) and coated onto either PET films or inorganic glass plates using a bar coating method. UV-3701 contains functionalized acrylic monomers and oligomers, besides the polymerization initiator, to form an acrylic coating layer upon UV illumination by a radical polymerization reaction. The coated films and glass plates were dried at 70°C for 1 min and illuminated with a high-pressure mercury lamp at UV intensity 76

S. Bhandarkar—contributing editor

Manuscript No. 23953. Received November 8, 2007; approved April 23, 2008.

[†]Author to whom correspondence should be addressed. e-mail: Kenji_adachi@ni.smm.co.jp

mW/cm² and belt speed 3 m/min, with a total UV energy of 146 mJ/cm². The dried coating thickness was evaluated using an Optical Profiler (Model NewView6200, Zygo Corp., Middlefield, CT) as well as by optical microscopy of cross sections. The amount of filler particles per unit projected area of the coated films/glasses (g/m²) was evaluated by precise weight measurements of the coated and uncoated films and glass plates. This quantity is more convenient than dried thickness in the particulate system because thickness can be varied easily by changing the filler-to-resin ratio while maintaining the same filler amount. The optical response of the coatings was measured using a spectrophotometer (Model U-4000, Hitachi High-Technologies Corp., Minato-ku, Tokyo, Japan), giving outputs of transmittance and reflectance profiles in the UV, visible, and infrared ranges (200–2600 nm), and yielding visible light transmittance (VLT), solar transmittance (ST), haze, Hunter's chromatic index, etc. ST is a total directly transmitted solar energy between 280 and 2500 nm (ISO-9050), given by

$$ST = \frac{\sum_{\lambda=280 \text{ nm}}^{2500 \text{ nm}} S(\lambda)T(\lambda)\Delta\lambda}{\sum_{\lambda=280 \text{ nm}}^{2500 \text{ nm}} S(\lambda)\Delta\lambda} \quad (1)$$

where $S(\lambda)$ is the spectral distribution of the solar radiation, $T(\lambda)$ is the spectral transmittance, and $\Delta\lambda$ is an increment of wavelength. ST can be a measure of the solar control property when compared at constant VLT.

III. Results and Discussion

(1) Optical Profiles of LaB₆-Dispersed Films and Dispersions

Figure 1 shows the transmittance and reflectance profiles of LaB₆-dispersed coatings of different thicknesses formed on a PET film substrate. A dispersion of 1.85 wt% LaB₆ milled to a dispersion particle size of 18 nm has been mixed with the UV-setting resin UV-3701 at a weight ratio of 1:1 and bar coated on PET films. The thickness of the coatings has been varied using bar rods of different diameters. The corresponding dried thickness varied between 4.8 and 28.2 μm. Measured amounts of LaB₆ in a unit-projected area of the coatings are shown in Fig. 1. The coated films are tinted green but are highly transparent, with haze values generally <2%. Strong absorption at around 1000 nm is observed for every film while showing a large selected transmittance at the visible wavelengths between 380 and 780 nm. This apparent absorption is obviously not related to an interference effect because it shows no thickness dependence. The reflectance of these coated films is low and varies between 3.7% and 7.7% throughout the measured wavelengths, where most of the reflected light on each of the nanoparticle surfaces is con-

sidered to be dumped out in the coating due to multiple reflections and absorption by the nanoparticles. An appreciable amount of reflectance 20%–30% could, however, be observed at 1100–2000 nm, when LaB₆ nanoparticles are much more densely packed in the coating, by eliminating the UV-setting binders.

The apparent absorption at around 1000 nm in Fig. 1 actually involves both absorption and scattering at the present particle size,^{4,5} and is generally called extinction. Although the precise value of the scattering component using a large integrating sphere will be reported in a separate paper,¹¹ we may note here that the scattering contribution is estimated as a small percentage considering the low haze value of <2% of those coating films.

Using a LaB₆ dispersion of known concentration held in a glass cell 12 mm × 12 mm × 44 mm (internally 10 mm × 10 mm × 43 mm) in size transmittance profiles similar to those shown in Fig. 1 have been obtained to calculate the molar extinction coefficient of LaB₆ particles, applying Lambert–Beer's law by $\log(I/I_0) = \epsilon cd$, where I_0 is the intensity of incident light, I is the intensity of transmitted light, d (cm) is the optical length (equals unity in the present case), and c is the concentration of LaB₆ nanoparticles in dispersion. A molar concentration $M = \text{mol/L}$ of LaB₆ in dispersion is used for c , where the molar quantity of the crystal lattice is defined as Avogadro's number of the LaB₆ unit cell.

The result, Fig. 2, shows a remarkable absorption capability of LaB₆. A major absorption peak is observed at 970 nm and a second largest peak at 300 nm, besides a small shoulder that is appreciable at around 700 nm in the major peak.

The origin of the main absorption at 970 nm is presumed to be an activated surface plasmon polariton of free electrons, because there are no interband transitions observed in the vicinity of 970 nm (1.278 eV) in the optical conductivity spectrum of LaB₆ reported by Kimura *et al.*¹² LaB₆ is a superior conductor with high carrier density $0.9 \times 10^{22} \text{ cm}^{-3}$, specific resistivity $1.5 \times 10^{-5} \Omega \cdot \text{cm}$, and mobility $33.1 \text{ cm}^2 \cdot (\text{V} \cdot \text{s})^{-1}$.¹³ The plasma edge is measured as 1.97 eV^{14} or 629 nm, which is close to the observed absorption peak at 970 nm. The second largest peak observed at 300 nm in Fig. 2 is considered to correspond to the interband transition, because Kimura *et al.*¹² detected a peak in the optical conductivity profile at 3.5 eV (354 nm), which they attributed to the interband transition from the B 2s, 2p bonding orbital to the unoccupied state in the conduction band. The small shoulder at 700 nm will be considered in a later section.

In order to compare the strength of the LaB₆ absorption, optical measurements were conducted for the well-known ITO

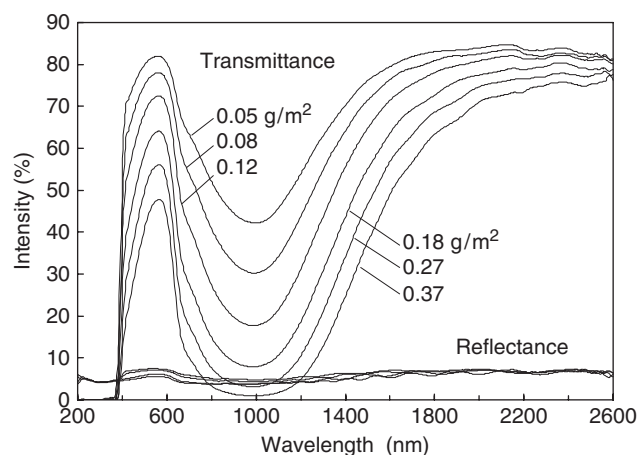


Fig. 1. Transmittance and reflectance profiles of LaB₆ nanoparticle-dispersed acrylic coatings with different thicknesses on PET films. The number of LaB₆ particles determined in a unit-projected area of the coatings is indicated.

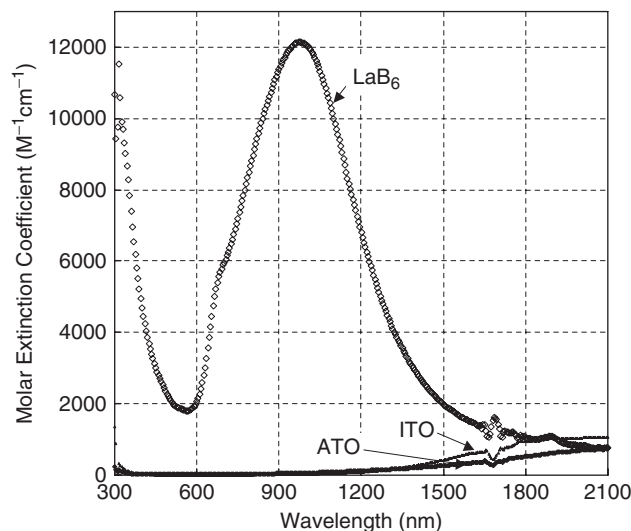


Fig. 2. Molar extinction coefficients of nanoparticle dispersions of LaB₆, tin-doped indium oxide (ITO), and antimony-doped tin oxide (ATO). The disturbance at wavelengths between 1620 and 1790 nm is due to absorption by toluene.

and ATO nanoparticle dispersions with dispersion particle sizes 18 and 12 nm, respectively. The NIR absorption in continuous ITO and ATO films has been attributed to the surface plasmon excitation that was experimentally detected by electron energy loss spectroscopy.¹⁵ The maximum extinction coefficients of LaB₆ and ITO at the respective peaks read $12\,142\text{ (M}\cdot\text{cm)}^{-1}$ at 975 nm and $1065\text{ (M}\cdot\text{cm)}^{-1}$ at 2075 nm, respectively. The peak height of LaB₆ is observed as an order of magnitude larger than that of ITO, clearly suggesting that LaB₆ could absorb NIR waves more strongly than ITO and ATO. This difference is considered to be related to the much higher carrier concentration of $0.9 \times 10^{22}\text{ cm}^{-3}$ in LaB₆¹³ as compared with $10^{20-21}\text{ cm}^{-3}$ in ITO¹⁶ and $10^{19-20}\text{ cm}^{-3}$ in ATO¹⁶. The high strength of the absorption property of LaB₆ should provide significant material and cost advantages over ITO and ATO.

(2) NIR Absorption of Rare-Earth Hexaborides

Trivalent rare-earth elements are known to form hexaborides that have similar free electron plasmon energies such as at 1.97 eV for LaB₆, 1.96 eV for CeB₆, 1.89 eV for PrB₆, 1.90 eV for NdB₆, and 1.90 eV for GdB₆, according to Kimura *et al.*¹⁴ Thus, nanoparticles of various rare-earth hexaborides were examined for capability of NIR absorption. Dispersions of LaB₆, CeB₆, PrB₆, NdB₆, and GdB₆ were prepared with polymer dispersants in toluene, and their transmittance profiles are shown in Fig. 3. This figure clearly indicates that the absorption valley around 1000 nm is a common characteristic of these rare-earth hexaboride nanoparticles. They are all milled to a similar particle size so as not to affect the optical response significantly. The peak transmittance around 550 nm has been made equal by adjusting the filler concentration in order to compare the size of the absorption valleys around 1000 nm in Fig. 3. The depth of the valleys is found to decrease in the order of LaB₆, CeB₆, PrB₆, NdB₆, and GdB₆.

The ionic radius of La, Ce, Pr, Nd, and Gd and the lattice constants of their hexaborides show a tendency to decrease in this order as the number of 4*f* electrons is increased (lanthanoid contraction). Roughly proportional to this contraction, the magnitude of the NIR absorption, as evaluated by the difference between the peak and bottom transmittances, is found to decrease as shown in Fig. 4.

In the hexaboride structure of the space group *Pm3m*, each rare-earth atom is surrounded by 24 nearest-neighbor boron atoms at an equal distance. The nearest-neighbor distance increases as the number of 4*f* electrons in rare-earth elements increases, and this is assumed to decrease the overlap of electron clouds of rare-earth 5*d* with boron 2*p* that form the conduction bands and are considered to reduce the density and mobility of free electrons. Because the origin of the NIR absorption is assumed to involve free electron plasmons, the largest NIR absorption of LaB₆ among the rare-earth hexaborides, as

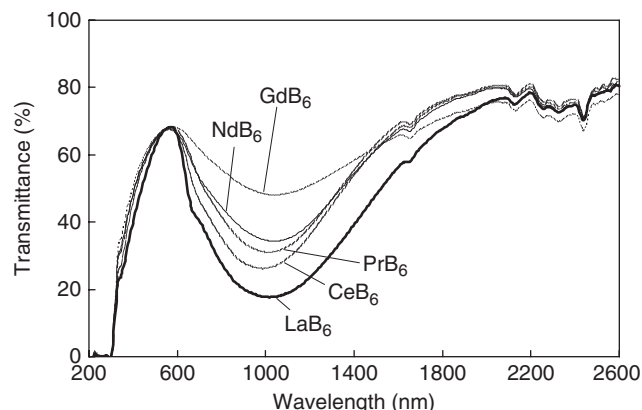


Fig. 3. Transmittance profiles of rare-earth hexaboride nanoparticle dispersions. The peak transmittance at 580 nm is set equal to compare the near infrared absorption around 1000 nm.

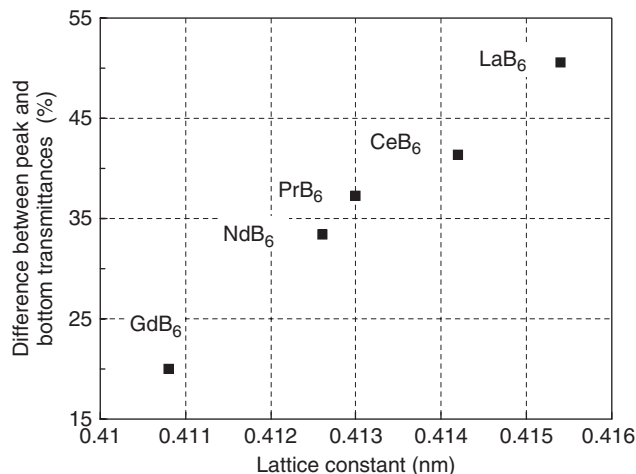


Fig. 4. Near infrared absorption of rare-earth hexaboride nanoparticles with regard to their lattice constants.

observed, is considered to be derived from the largest ionic radius of La and the corresponding largest overlap of electron clouds.

This interpretation has been extended to alkaline-earth hexaborides such as BaB₆, SrB₆, and CaB₆, with lattice parameters 0.4275, 0.4200, and 0.4145 nm, respectively, which are larger than or comparable to 0.4154 nm of LaB₆. NIR absorption was observed with BaB₆, SrB₆, and CaB₆ nanodispersions, but not as strong as with lanthanum hexaboride. This suggests that the valence two alkaline-earth elements such as Ba, Sr, and Ca do not form a large overlap of electron clouds with boron 2*p* as were formed with the valence three rare-earth elements in the structure of hexaboride.

Kimura *et al.*¹⁴ found a small additional absorption structure at 0.6 eV (2066 nm) in the optical conductivity profiles of all the rare-earth hexaborides except for LaB₆. They ascribed this absorption to the 4*f* electrons, and have shown that with increasing number of 4*f* electrons, the effective electron number related to this absorption, N_{IR} , increases while that related to the Drude absorption, N_D , decreases. While the present observation did not detect any absorption peaks at 2066 nm, the 970-nm absorption is observed to decrease with increasing number of 4*f* electrons, and thus appears to reflect only N_D among the total conduction electrons $N_D + N_{IR}$.

(3) Fine Structure and Diffraction Results

The crystal structure of the as-produced LaB₆ powder was confirmed both by X-ray diffraction (XRD) and by electron diffraction to be of the cubic CaB₆ type. Each as-produced LaB₆ particle was polycrystalline as observed by TEM. A well-dispersed LaB₆ dispersion in toluene, prepared after 28 h in a paint shaker mill, was observed both by TEM (Fig. 5) and by XRD (Fig. 6(a)). Fine particles between a few nanometers and 100 nm in size can be observed in Fig. 5. Numerous fine particles smaller than 30 nm are involved, although these smaller particles tend to lose a high contrast probably due to the presence of a high-polymer dispersant in the matrix. These LaB₆ nanoparticles in well-dispersed solutions have been found mostly as single crystalline particles, as illustrated in Fig. 7 by the lattice fringe image and the corresponding microbeam electron diffraction pattern. Particle shape is deviated from a sphere because they are debris from the collisions with YTZ beads during the milling process. Fine particles observed in Fig. 5 are found as, actually, a mixture of LaB₆ and ZrO₂ particles because zirconia beads are also crushed on the surface. YTZ beads are initially of a tetragonal phase of partially stabilized zirconia, but as they are subjected to strong shearing and tearing forces during the milling process with an increased surface temperature estimated to be up to 800°–1000°C, a part of the tetragonal phase is inferred to trans-

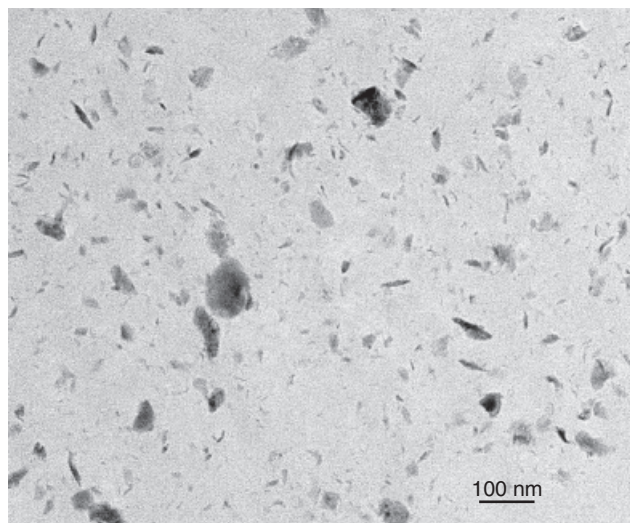


Fig. 5. Transmission electron microscopy bright field image of a LaB_6 nanoparticulate dispersion in toluene with a high-polymer dispersant.

form into the monoclinic phase martensitically. Both tetragonal and monoclinic ZrO_2 reflections can be identified in the XRD pattern in Fig. 6(a). It is possible to distinguish ZrO_2 particles by the dark-field technique using diffraction rings derived from ZrO_2 , which shows that the size and shape of LaB_6 and ZrO_2 particles are similar.

A typical particle size distribution measured by UPA-150 is shown in Fig. 8 for a LaB_6 dispersion dispersed in a paint shaker mill for 28 h. Most of the particles are between 10 and 30 nm in size with the peak maximum at 15.2 nm, while many larger particles form a tail up to 150 nm. This tailing was more or less a common characteristic observed for the bead-milled nano-dispersions.

Figure 9 shows how the average LaB_6 particle size is decreased during the milling process when ZrO_2 particles are introduced. The average dispersion particle size shows good agreement with the Scherrer crystallite size except for the first measurement, indicating that the well-dispersed nanosized particles are single crystalline, in agreement with the TEM observation. The ZrO_2 weight ratio with respect to LaB_6 , determined

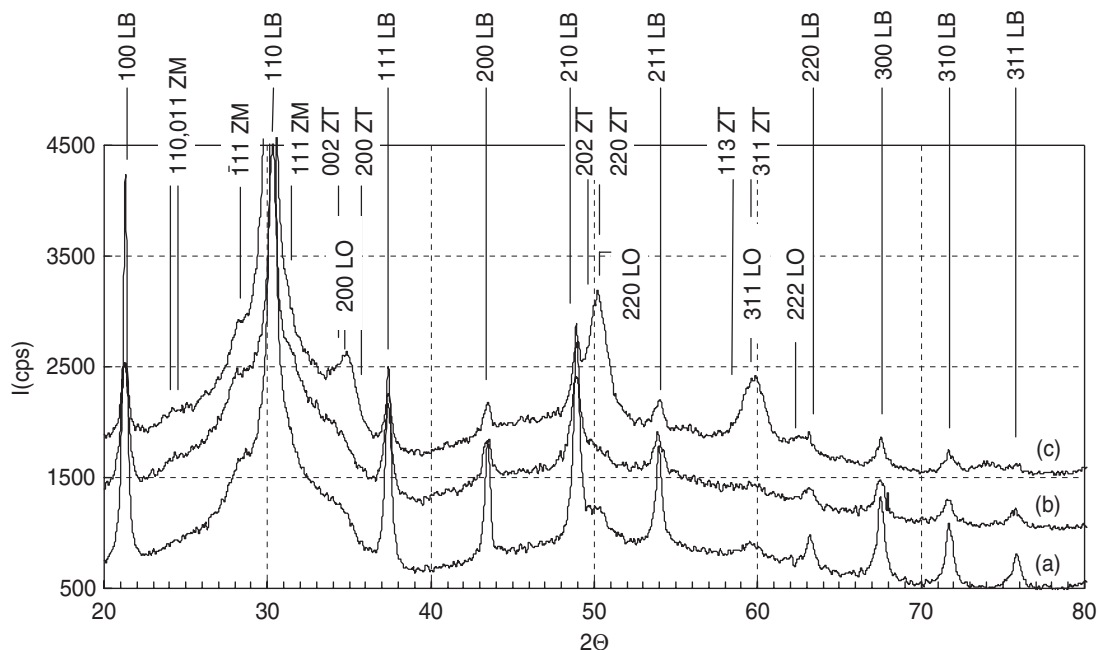


Fig. 6. X-ray diffraction patterns of LaB_6 powders with dispersion particle size 18 nm (a), 13 nm (b), and the powder (b), further heated in a N_2 atmosphere at 500°C for 1 h (c). LB, ZM, ZT, and LO denote LaB_6 , monoclinic ZrO_2 , tetragonal ZrO_2 , and LaO phases, respectively.

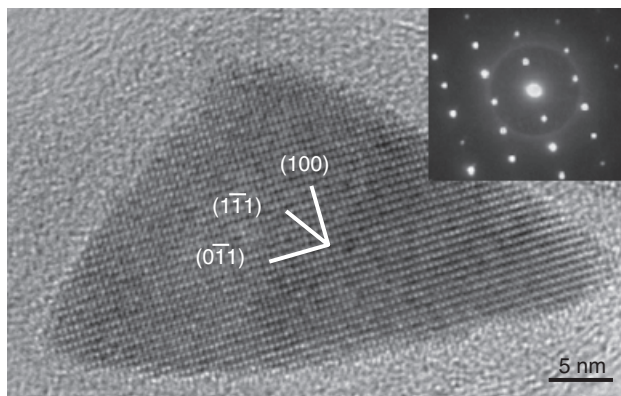


Fig. 7. High-resolution transmission electron microscopic image of a single LaB_6 nanoparticle in the $[011]$ direction with the corresponding microbeam diffraction pattern.

by inductively coupled plasma spectrometry, increases from 0 to 2.9 in 82 h. This significant incorporation of ZrO_2 particles into the dispersion does not, however, lead to much modification of the optical response of films, as shown in Fig. 10. In order to assess the optical effect of ZrO_2 contamination, ZrO_2 nanoparticulate dispersion was separately prepared by milling the coarse powder of partially stabilized tetragonal ZrO_2 with the dispersant in toluene, down to the same size as the LaB_6 dispersion. ZrO_2 dispersion is shown to be almost inert optically in the visible range. Figure 10 gives a calculated transmittance profile of pure LaB_6 dispersion, obtained by subtracting the ZrO_2 contribution from the measured spectrum of LaB_6 dispersion containing ZrO_2 at a ratio of $\text{ZrO}_2/\text{LaB}_6 = 1.6$. This indicates that the presence of ZrO_2 particles leads to some 5.2%–12.4% underestimate of LaB_6 transmittance in the visible range but can be significant in the UV range, e.g., 46.5% underestimate at 300 nm, although the overall characteristic of the profile remains the same.

(4) Effect of Particle Size on Optical Properties

The absorption property of LaB_6 as shown in Fig. 2 is a response of the electromagnetic wave passing through a thin two-dimensional layer containing homogeneously distributed

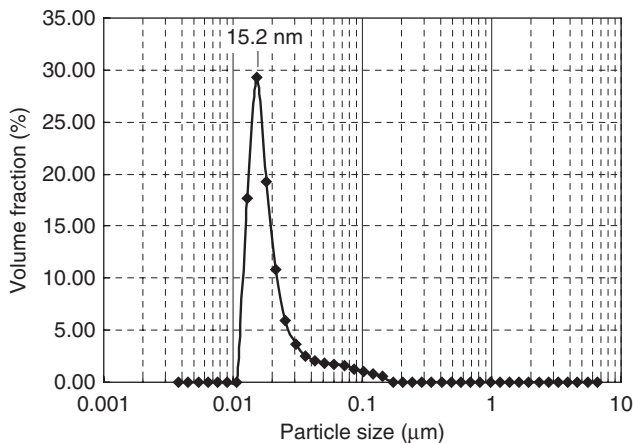


Fig. 8. Particle size distribution of a LaB₆ dispersion of average particle size 15.6 nm milled by a paint shaker mill for 28 h.

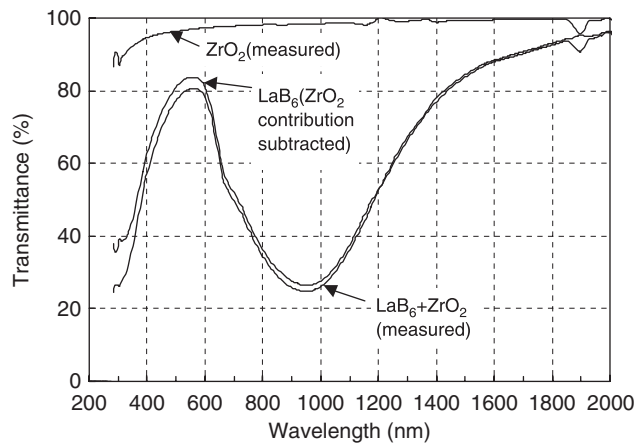


Fig. 10. Refinement of transmittance profiles by excluding ZrO₂ contribution. See text for details.

nanosized LaB₆ particles. It is pointed out⁴ that the important variables to determine the absorption profile and peak wavelength are basically the particle size and shape, and also the refractive index of the surrounding matrix. Therefore, the effect of particle size on optical properties has been examined below.

Figure 11 shows the ST of LaB₆ dispersions, plotted as a function of average dispersion particle size. Because ST depends on VLT, the LaB₆ concentration was finely adjusted to have a constant VLT at 70%. ST is found to show a minimum at around 20–30 nm in Fig. 11, indicating that the best solar control property with LaB₆ dispersions is given in this limited particle size range.

Figure 12 shows a variation of transmittance profiles of LaB₆ dispersion liquids containing a constant concentration, 0.004 wt%, of LaB₆ at various particle sizes between 13 and 120 nm. The shapes of the profiles are found to be significantly different. Transmittance generally decreases at particle sizes from 120 to 18 nm, while it tends to increase from 18 to 13 nm. Molar extinction coefficients have been calculated from these optical data to show the particle size dependence as shown in Fig. 13. An initial decrease in the particle size from the coarse 120 nm intensifies the extinction coefficient, where the largest extinction coefficient is observed as 13 500 (M · cm)⁻¹ for particle sizes of 18 and 26 nm. Further decrease in particle size then slightly weakens and shifts the extinction coefficient toward the longer wavelength while further emphasizing the shoulder at 650 nm.

On decreasing the particle size from 120 to 18 nm, a high-transmission region in the visible range becomes more widely

transmitting, while an absorbing region in the NIR range becomes more absorptive. The expansion of the visible range is considered to be due to the much more rapid decrease in scattered light at shorter wavelengths than at longer wavelengths, following Rayleigh's formula. The increase in absorption at 970 nm on decreasing the particle size is interpreted from the two aspects—a decreasing absorption capability of single nanoparticles and an increasing number of nanoparticles involved in the total absorption. The absorption cross section clearly decreases with decreasing particle size, as demonstrated for silver colloids,¹⁷ while the number of particles involved increases by the power of three when a filler weight concentration is kept constant in liquid. When the radius of the particle is reduced from r to r/p at a constant weight concentration, the total absorption, as it is proportional to the total projected area of the whole particles, increases from πr^2 to $\pi(r/p)^2 \times p^3 (= p\pi r^2)$, and therefore the total absorption is expected to increase by a factor of p . Assuming that the size dependence of the absorption cross section is smaller than p , the 970-nm absorption is expected to increase as observed in Fig. 13. A more quantitative account of this change based on the Mie theory calculations will be given elsewhere.¹¹

At particle sizes of 18 nm and below, profiles in the visible range show little change, in contrast to the NIR profile that grows a shoulder at around 700 nm into a subpeak in Fig. 12. This subpeak corresponds to the small absorption peak at 650 nm in Fig. 13. Figure 6 shows that on decreasing particle size from (a) 18 nm to (b) 13 nm, a subtle formation of LaO

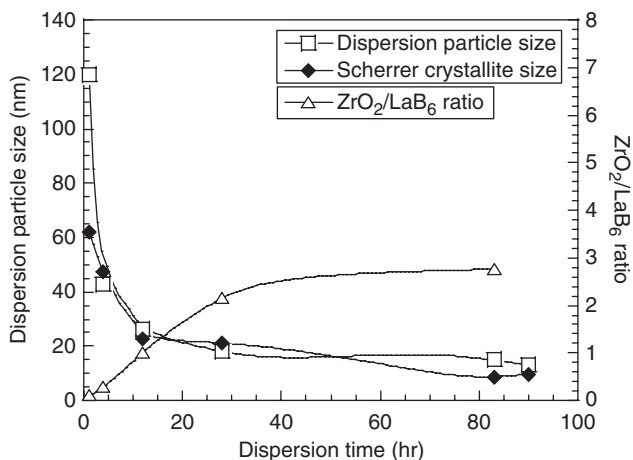


Fig. 9. Changes in dispersion particle size, Scherrer crystallite size, and ZrO₂ contamination with dispersion time in a paint shaker mill with YTZ media beads.

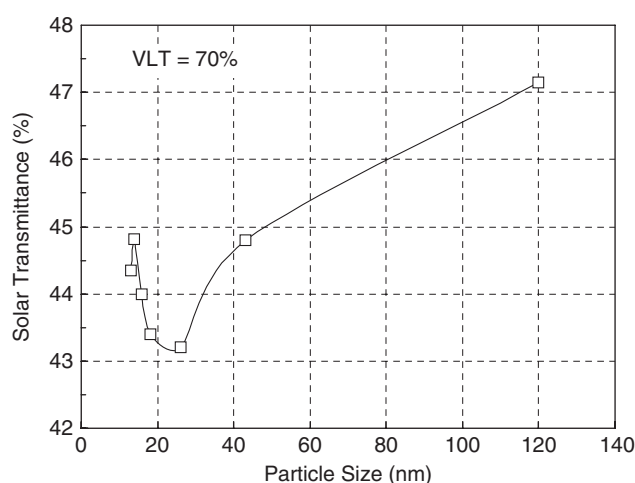


Fig. 11. Effect of dispersion particle size on solar transmittance property at a constant visible light transmittance of 70%.

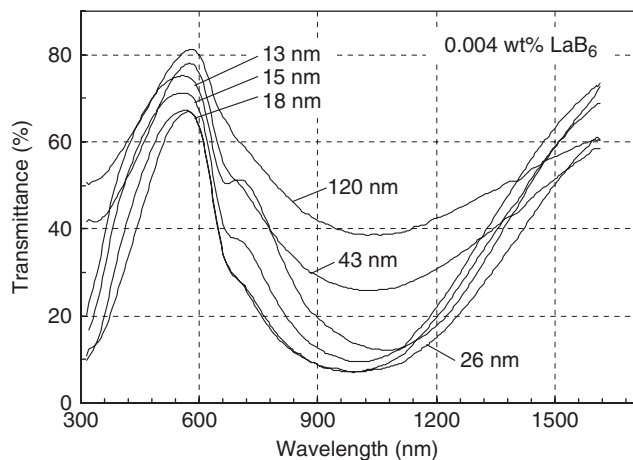


Fig. 12. Transmittance profiles of LaB_6 dispersions of constant concentration at 0.004 wt% with different particle sizes.

is suggested from the patterns. The LaO peaks (200), (220), and (311) grew more appreciably in the XRD pattern (c) when the 13 nm LaB_6 dispersion was slowly heated to evaporate solvent toluene and further heated at 500°C for 1 h in the nitrogen atmosphere. LaO has been reported to be synthesized at $800^\circ\text{--}1000^\circ\text{C}$ under high pressure, and has a metallic property with a positive TCR and a high conductivity of $2.7 \times 10^{-4} \Omega \cdot \text{cm}$ at room temperature.¹⁸ Therefore, it is well speculated that either an interband transition or a plasmon resonance could take place in LaO to produce a small additional absorption at 650 nm. The presence of tiny LaO crystallites has actually been observed by a TEM dark field technique in LaB_6 aggregates obtained by evaporating toluene and heating in air at 200°C for 1 h.

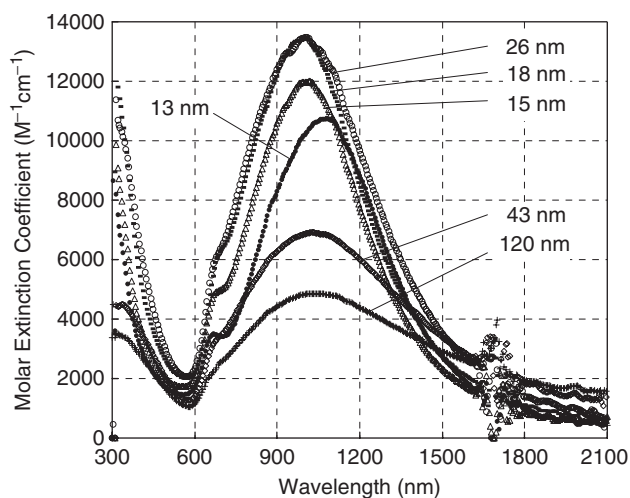


Fig. 13. Molar extinction coefficients of LaB_6 dispersions of different particle sizes between 120 and 13 nm. The disturbance at wavelengths between 1620 and 1790 nm is due to absorption by toluene.

IV. Conclusions

Rare-earth hexaboride nanoparticle dispersions have been prepared in solvent toluene with organic dispersants using a media agitation mill with zirconia beads. The nano- LaB_6 dispersions as well as their coatings cured with acrylic binders have been shown to exhibit a strong NIR absorption with a high VLT. The major absorption at 970 nm is assumed to be due to the free electron surface plasmon resonance, and other rare-earth hexaborides CeB_6 , PrB_6 , NdB_6 , and GdB_6 having a similar plasma edge are confirmed as exhibiting the same effect. The molar extinction coefficient of LaB_6 nanoparticulate dispersion is found to be at least an order of magnitude larger at the main peak than that of ITO dispersions, showing a high potential as an economical solar control material. On decreasing the dispersion particle size from 120 to 18 nm, both VLT and NIR absorption are increased to enhance the solar control property, while from 18 to 13 nm a part of LaB_6 was found to decompose appreciably into LaO, which degrades the solar control property and gives rise to an additional absorption around 650 nm. The ZrO_2 contamination is optically not active and exerts only a minor effect on the optical properties of rare-earth hexaboride dispersions.

References

1. Hamberg and C. G. Granqvist, "Evaporated Sn-Doped In_2O_3 Films: Basic Optical Properties and Applications to Energy-Efficient Windows," *J. Appl. Phys.*, **60** [11] R123–59 (1986).
2. A. Nishihara, T. Hayashi, and M. Sekiguchi, "Infrared Ray Cutoff Material and Infrared Cutoff Powder Use for Same", US Patent No. 5518810, 1996.
3. M. Saito, "Transparent Heat Ray Shielding Materials by ATO Ultrafine Particles," *Convertec*, **25** [7] 1–5 (1997) (in Japanese).
4. C. F. Boren and D. R. Huffman, *Absorption and Scattering of Light by Small Particles*. Wiley Interscience, New York, 1983.
5. U. Kreibitz and M. Vollmer, "Optical Properties of Metal Clusters"; p. 25 in *Springer Series in Materials Science*, Vol. 25, Edited by J. P. Toennies. Springer-Verlag, New York, 1995.
6. H. Kuno, H. Takeda, and K. Adachi, "Coating Solution for Forming a Selectively Transmitting Film, a Selectively Transmitting Film and a Selectively Transmitting Multilayer Film," US Patent No. 6060154, 2002.
7. H. Kuno, H. Takeda, and K. Adachi, "Film for Cutting Off Heat Rays and a Coating Liquid for Forming the Same," US Patent No. 6277187, 6221945, 2001.
8. K. Adachi, H. Takeda, and H. Kuno, "Solar Heat Shielding Functional Films Using Nanoparticles"; pp. 10–5, *Proceedings of the 69th Meeting of the Japanese Society for the Promotion of Science*, July 9–10, Nagoya, 2002.
9. K. Fisher, "Polyvinylbutyral Blends with Lanthanum Hexaboride for Use in Laminated Solar Control Glazing"; pp. 110–113, *Proceedings of Glass Processing Days 2005*, June 17–20, Tampere, 2005.
10. F. S. Galasso, *Structure and Properties of Inorganic Solids*, Chapter 3.4. Pergamon Press Inc., Oxford, 1970.
11. T. Asahi, M. Miratsu, and K. Adachi, unpublished research, (2008).
12. S. Kimura, T. Namba, M. Tomioka, S. Kunii, and T. Kasuya, "Electronic Structure of Rare-Earth Hexaborides," *Phys. Rev. B*, **46** [19] 12196–204 (1992).
13. Yu. B. Paderno and G. V. Samsonov, "The Electric Properties of the Hexaborides of Alkali-Earth and Rare-Earth Metals and Thorium (in Russian)," *Doklady Akad. Nauk USSR*, **137** [3] 646–7 (1961).
14. S. Kimura, T. Namba, S. Kunii, T. Suzuki, and T. Kasuya, "Anomalous Infrared Absorption in Rare-Earth Hexaborides," *Solid State Commun.*, **75** [9] 717–20 (1990).
15. P. A. Cox, W. R. Flavell, and R. G. Egdell, "Solid-State and Surface Chemistry of Sn-Doped In_2O_3 Ceramics," *J. Solid State Chem.*, **68**, 340–50 (1987).
16. K. L. Chopra, S. Major, and D. K. Pandya, "Transparent Conductors—A Status Review," *Thin Solid Films*, **102**, 1–46 (1983).
17. D. D. Evanoff Jr and G. Chumanov, "Size-Controlled Synthesis of Nanoparticles. 2. Measurement of Extinction, Scattering and Absorption Cross Sections," *J. Phys. Chem. B*, **108** [37] 13957–62 (2004).
18. J. M. Leger, P. Aimonio, J. Loriers, P. Dordor, and B. Coqblin, "Transport Properties of SmO ," *Phys. Lett.*, **80A** [4] 325–7 (1980). □